Influence of Metal Transfer Behavior Under Ar And CO_2 Shielding Gases On Geometry And Surface Roughness of Single And Multilayer Structures In GMAW-Based Wire Arc Additive Manufacturing of Mild Steel

Mitsugu Yamaguchi (yamaguchi@se.kanazawa-u.ac.jp)
Advanced Manufacturing Technology Institute, Kanazawa University https://orcid.org/0000-0001-6034-3089

Rikiya Komata
Kanazawa University

Tatsuaki Furumoto
Kanazawa University

Satoshi Abe
Kanazawa University

Akira Hosokawa
Kanazawa University

Research Article

Keywords: Wire arc additive manufacturing, Gas metal arc welding, Metal transfer behavior, Mild steel, Shielding gas

Posted Date: July 12th, 2021

DOI: https://doi.org/10.21203/rs.3.rs-657956/v1

Version of Record: A version of this preprint was published at The International Journal of Advanced Manufacturing Technology on November 11th, 2021. See the published version at https://doi.org/10.1007/s00170-021-08231-8.

Abstract

Wire arc additive manufacturing (WAAM) is advantageous for fabricating large-scale metallic components, however, a high geometric accuracy as that of other AM techniques cannot be achieved because of the deposition process with a large layer. This study focuses on the WAAM process based on gas metal arc welding (GMAW). To clarify the influence of shielding gas used to protect a molten metal during fabrication on the geometric accuracy of the built part obtained via the GMAW-based WAAM process, the influence of the metal transfer behavior on the geometry and surface roughness of the fabricated structures was investigated via visualization using a high-speed camera when single and multilayer depositions were performed under different heat inputs and gases. However, when using Ar gas, the heat flux from an arc to the workpiece is relatively low, limiting the depth of the molten pool during welding. The effect of its characteristics on the stair steps that are inevitably produced on the side face of the multilayer structure in the WAAM process was verified, and for a heat input of 1.17 kJ/cm under Ar gas, a higher geometric accuracy of the multilayer structure was obtained without interlayer cooling. The short circuit between the metal droplet and the fabricated surface, where the molten pool is insufficiently formed, resulted in a hump formation. Further, the metal transfer under Ar gas reduced the surface irregularities on the fabricated structure.

Introduction

Wire arc additive manufacturing (WAAM) is categorized as a directed energy deposition (DED) technique that is specifically developed for fabricating large-scale metallic components with complex features [1]. Compared with other AM techniques, WAAM is advantageous because of its high efficiency, high material usage, and low cost. Moreover, owing to its applicability to a variety of materials, this technique has been extensively employed in the aerospace, automotive, and rapid tooling industries [2, 3]. In the WAAM process, metallic components are produced when an electrical arc melts a wire-based feedstock and deposits it layer-upon-layer. Typically, gas metal arc welding (GMAW), gas tungsten arc welding (GTAW), and plasma arc welding (PAW) are applied in this process [4]. WAAM enables high-density and superior mechanical properties of the components [5, 6]. However, the quality of the WAAM-fabricated components is inadequate to satisfy the general industrial applications because of disadvantages such as residual stress and distortion from excessive heat input [7-9]. Specifically, although the components have simple geometries, the geometric accuracy is not comparable to that of other AM techniques [10]. Owing to the deposition process with a large layer, stair steps are inevitably produced on the side face of the components. This can significantly affect not only the surface quality of the components, but also the removal volume of materials in the finish machining process. Therefore, improving the surface quality is a key challenge in WAAM.

The surface quality of the WAAM-fabricated structures depends on several key parameters. Previous studies have reported certain factors that can affect the surface quality of the fabricated structures. Xiong et al. [11] investigated the influence of the interlayer temperature, traveling speed, wire feed speed, and constancy of the ratio of the wire feed speed to the traveling speed on the surface roughness of thin-

wall parts fabricated using H08Mn2Si steel and reported that the surface quality of the thin-walled parts improved with the decrease in the interlayer temperature. Further, when the ratio of the wire feed speed to the traveling speed was constant, the surface roughness increased with an increase in the wire feed speed. In addition, the surface roughness decreased with a reduction in the wire feed speed and traveling speed. Prado-Cerqueira et al. [12] applied the cold metal transfer (CMT) advanced technique in the WAAM process, which was developed to prevent excessive heat input by controlling the wire feed speed and polarity. It was concluded that the simple CMT without polarity change improved the homogeneous hardness distribution, mechanical strength, and surface quality of the thin-wall parts fabricated using mild steel. Further, a shielding gas also plays an important role in the WAAM process in controlling the layer geometry, deposition rate, and spatter generation. Jurić et al. [13] prepared four types of shielding gases (97.5% Ar + 2.5% CO_2, 95.5% Ar + 3% He + 1.5% H_2, 95% Ar + 5% H_2, 99.999% Ar) and compared the root-mean square height (S_q), arithmetic mean height (S_a), and mechanical properties of the specimens of Inconel 625 fabricated under each shielding gas. This revealed that 97.5% Ar + 2.5% CO_2 shielding gas resulted in higher hardness and tensile strength of the specimens, but poor surface quality. Silwal et al. [14] focused on the WAAM process based on the surface tension transfer (STT) technique, and investigated the influence of the Ar and CO_2 shielding gas mixture on the dimensional accuracy, mechanical properties, and microstructure of the wall structure fabricated using mild steel revealing that the higher CO_2 content led to higher melt pool temperatures, whereas the lower CO_2 content resulted in a dimensionally accurate geometry.

The first classification of metal transfer modes in GMAW was established by the International Institute of Welding (IIW) in 1976 [15]. Subsequently, the effects of the welding process parameters on the metal transfer mode have been researched. Scotti et al. [16, 17] investigated the metal transfer behavior of carbon steel under different combinations of welding current, voltage, and gas composition and concluded that there were three classes of metal transfer modes: natural metal transfer, controlled metal transfer, and interchangeable metal transfer. For the natural metal transfer, two types of metal transfer modes, contact droplet transfer and free-flight droplet transfer to the weld pool, were observed. Further, the controlled metal transfer consisted of improved natural modes to obtain better process characteristics, such as spatter minimization, weld geometry control, and heat input stabilization. The interchangeable metal transfer was a mixed mode that consisted of two or more natural transfer modes. Teixeira et al. [18] observed the metal transfer behavior of mild steel under five types of shielding gases (Ar, Ar + 2% O_2, Ar + 10% CO_2, Ar + 25% CO_2, and CO_2) in GMAW. Metal transfer mode maps were plotted to identify the regions of each type of metal transfer revealing that the interchangeable globular/spray metal transfer was only obtained for Ar + 10% CO_2 and Ar gases. In contrast, the Ar + 25% CO_2 gas, owing to the high percentage of CO_2, the transition current increased, resulting in a more difficult change to spray transfer. In addition, the presence of oxygen in the Ar + 2% O_2 shielding gas resulted in smaller droplets than in pure argon. Furthermore, several studies have explored the impact of shielding gas on metal transfer behavior in the WAAM process. Wu et al. [19] investigated the influence of heat accumulation on bead formation, arc stability, and metal transfer behavior during the building of Ti6Al4V

in GTAW-based WAAM. It was concluded that the heat accumulation led to variations in the bead geometry, which resulted in variations in the arc shape and droplet transfer mode. Ríos et al. [20] focused on the metal transfer behavior in PAW-based WAAM. This revealed that the metal transfer could be classified into three modes, and stable transfer was obtained when the surface of the molten pool was convex. Further, Liang et al. [21] investigated metal transfer behavior in a GMAW-based WAAM and determined that the interaction between the arc voltage and arc current was the most important factor influencing droplet transfer. The droplet radius decreases exponentially with an increase in the frequency of droplet transfer, whereas the deposition rate increased with an increase in the frequency of droplet transfer.

These results show that it is important to control the heat input and the associated droplet transfer mode during the WAAM process. The mechanism of surface defect formation in the GMAW-based WAAM process and its relation to the geometric accuracy of the fabricated structure are being elucidated. However, the variation in the metal transfer behavior with the increase in the number of layers under different gases on the geometry and surface roughness of the multilayer structures has not been fully elucidated. Although CO_2 gas is a preferred shielding gas for the GMAW process of mild steels because it provides advantages such as higher welding speeds, greater penetration, and lower cost, its use is restricted because of problems associated with spattering and element losses due to oxidation. Meanwhile, it is known that Ar gas has a disadvantage in that the heat flux from an arc to the workpiece is relatively low, which limits the depth of the molten pool during welding [22]. Further, in the WAAM process, stair steps are inevitably produced on the side face of the multilayer structure, thus, the effect of the gas characteristics on the penetration and surface roughness is an important consideration.

This study focused on the GMAW-based WAAM process and addressed the following deficiencies. First, the metal transfer behavior during the building was observed under various heat inputs and shielding gases, such as Ar and CO_2. Second, the influence of the metal transfer behavior on the geometry and surface roughness of the single and multilayer structures was investigated. Finally, the chemical composition of the fabricated surface was analyzed using energy-dispersive X-ray spectroscopy (EDS). In the WAAM process, the cost of shielding gas cannot be ignored owing to the long processing time required to fabricate large-scale metallic components. In view of constantly increasing prices, the use of an expensive gas mixture can be avoided using a cheaper gas [23]. Furthermore, the process parameter conditions that enable the elimination of interlayer cooling during the building are desired to improve the processing efficiency. Therefore, this study attempted to provide a simplified shielding gas selection process and verified the limitations of fabricating a thin-wall structure without interlayer cooling.

Materials And Procedures

Figure 1 illustrates the experimental setup, and Table 1 lists the experimental conditions. A combined processing machine (Yamazaki Mazak Corp., VARIAXIS j-600AM) composed of a welding power source (Fronius International GmbH, TPS 4000) and a 5-axis machining center was used. The GMAW technique with a constant voltage was applied in the WAAM process. A filler wire with a diameter of 1.2 mm was

mild steel (JIS Z 3312: YGW12), which was developed for welding under CO_2 gas. Further, a spool was loaded on the wire feeding system, and the filler wire was fed coaxially with the welding torch. In addition, CO_2 and Ar gases were supplied via a welding torch as a shielding gas. The substrate was carbon steel (AISI 1049) with dimensions of 150 mm × 150 mm × 20 mm.

Table 1
Fabricating conditions.

Process parameter		
Wire feed speed [m/min]	1.6	3
Current *I* [A]	63	127
Voltage *E* [V]	15.5	16.8
Traveling speed *v* [mm/min]	500	
Z pitch [mm]	1	
Number of layer	1, 2, 3, 5, 11, 31	
Shielding gas	CO_2, Ar	
Gas flow rate [L/min]	15	
Wire		
Material	Mild steel (JIS YGW12)	
Diameter [mm]	1.2	
Composition [wt%]	0.07 C, 0.49 Si, 1.02 Mn, 0.008 P, 0.016 S, Fe Bal.	
Substrate		
Material	AISI 1049 (JIS S50C)	
Dimension [mm] × [mm] × [mm]	150 × 150 ×20	

The voltage, current, and traveling speed are the primary parameters that can be adjusted. The heat input *Q* was calculated using the following equation [24]:

$$Q = \frac{U \times I \times 60}{v \times 1000}\ [\mathrm{kJ/cm}] \quad (1)$$

where *U* is the voltage, *I* is the current, and *v* is the traveling speed. The fabrication experiment was performed at various wire feed speeds (WFS). Further, the current and voltage changed with the WFS, which was controlled by the welding power source. The current and voltage were 63 A and 15.5 V at the WFS of 1.6 m/min, and 127 A and 16.8 V at the WFS of 3.0 m/min. When the traveling speed was 500 mm/min, the heat inputs were 1.17 kJ/cm and 2.56 kJ/cm, respectively. The current and voltage waveforms during the building were measured using a welding monitor (Aichi Sangyo Co., Ltd.,

ROB5000) equipped with a welding power source. The metal transfer behavior during the building was observed using a high-speed camera (Shodensha Co., Ltd., CHU530EX-B) that was fixed near the welding torch using a flexible arm, and the metal transfer behavior during the building was observed at a distance of 35 mm and an angle of 45° from the vertical direction. The frame capture rate was set at 1500 rpm with a resolution of 512 × 480 pixels. The traveling path of the welding torch is illustrated in Fig. 2. The distance between the contact tip and substrate was initially 15 mm. Subsequently, the torch moved 100 mm in the X direction and rose 1 mm in the Z direction. Thereafter, the torch was reversed in the -X direction, repeating these processes from one layer up to 31 layers without inter-layer cooling. The value of the Z pitch was determined through a preliminary experiment because the layer geometry depends on the fabrication conditions, such as the WFS and traveling speed [25]. A Z pitch of 1 mm was selected from the average value of the height of the single layer at a heat input of the 1.17 kJ/cm. Further, the height and width of the single and multilayer structures were measured using a laser scanner (OPTEX FA Co., Ltd., LS-100CN). This was performed by irradiating a line laser with a width of 27 mm on the single and multilayer structures at 10 points to obtain the surface geometry. A schematic of the surface roughness measurement is shown in Fig. 3. In this study, the laser vision measurement based on the least squares method was adopted from the studies of Xiong et al. [11, 26]. The surface roughness of the side face of the thin-walled structures with 31 layers was evaluated. The structures had a length and height of approximately 100 and 25 mm, respectively. One specimen with dimensions of 20 mm × 20 mm was sectioned from the center area of each structure for the surface roughness measurement. Table 2 presents the measurement conditions for surface roughness. The chemical composition of the fabricated surface was analyzed using energy-dispersive X-ray spectrometry (JEOL Ltd., JSM-7100F).

Table 2
Measuring conditions for surface roughness.

Frequency	Scanning speed	Reference resolution
[kHz]	[mm/s]	[μm]
10	3	25

Experimental Results

3.1. Observation of metal transfer behavior

Figure 4 shows one cycle of metal transfer behavior during the building. These high-speed images were observed in the 3rd layer deposition at the heat input of 2.56 kJ/cm under Ar gas. The arc was generated at the tip of the filler wire (Fig. 4a), which subsequently increased (Fig. 4b). Thereafter, a metal droplet formed at the tip of the wire (Fig. 4c). This was followed by a short circuit between the metal droplet and the molten pool (Fig. 4d). Subsequently, a liquid metal bridge was formed, and the droplet was sucked into the molten pool (Fig. 4e). Finally, the arc was reignited at the tip of the wire (Fig. 4f). These cycles were repeated during the building process.

3.2. Metal transfer behavior during single and multilayer deposition

Figure 5 demonstrates the variations in the current and voltage during the fabrication for 5 layers when the heat input was 1.17 kJ/cm under Ar gas. The current and voltage were set to 63 A and 15.5 V, respectively. The variations decreased as the number of layers increased to three or more, although it was markedly large in the 1st and 2nd layers.

Figure 6 displays the high-speed images of the metal transfer behavior in the 1st layer deposition for a heat input of 1.17 kJ/cm under Ar gas. The arc was generated at the tip of the wire after the droplet detachment (Fig. 6a). Subsequently, a metal droplet was formed at the tip of the wire (Fig. 6b), which gradually increased in radius (Fig. 6c). The droplet was in contact with the substrate during the short-circuit phase (Fig. 6d). Thereafter, the arc was extinguished, and the tip of the wire was heated by Joule heating (Fig. 6e). Then, the wire was snapped off and the arc reignited simultaneously, and the detached droplet was left on the substrate (Fig. 6f). This is followed by the droplet formation.

Figure 7 shows the high-speed images of the metal transfer behavior in the 3rd layer deposition for a heat input of 1.17 kJ/cm under Ar gas. The arc is generated after the short-circuit phase (Fig. 7a). Subsequently, a metal droplet is formed at the tip of the wire. The arc blew to the surface of the molten pool in the traveling direction (Fig. 7b). The molten pool is constantly formed in front of the wire (Fig. 7c). Thereafter, a liquid metal bridge was formed, and the droplet was sucked into the molten pool (Fig. 7d). This was followed by arc regeneration and droplet formation (Fig. 7e, f).

3.3. Metal transfer behavior under different shielding gases

Figure 8 compares the metal transfer behavior for a heat input of 1.17 kJ/cm under different gases. These images were observed 9 ms after the short-circuit phase in the deposition of the 3rd layer. For Ar gas, the droplet radius is larger than that of CO_2 gas. The arc blew widely in the traveling direction under Ar gas, whereas it blew in the narrow area just below the wire under CO_2 gas. High-speed images with 7500 shots for 5 s were used to evaluate the frequency of the short circuit during the fabrication. Ar gas showed a frequency of 17.26 Hz, whereas CO_2 gas exhibited a frequency of 48.84 Hz. This indicates that CO_2 gas promotes the transfer of smaller droplets to the molten pool at a higher frequency.

Figure 9 depicts the variations in the current and voltage during the fabrication for 5 layers when the heat input was 1.17 kJ/cm under CO_2 gas. The variations in the current and voltage under CO_2 gas increased with an increase in the number of layers.

Figure 10 illustrates the high-speed images of the metal transfer behavior in the 31st layer deposition for heat input of 1.17 kJ/cm under CO_2 gas. The arc is generated after the short circuit phase (Fig. 10a). Thereafter, a droplet formed at the tip of the wire. In contrast to Ar gas, the arc blew to the surface of the molten pool in the traveling direction (Fig. 10b). The spot where the arc blew changed instantaneously from the molten pool to the previously fabricated surface (Fig. 10c). This was followed by a short circuit

between the droplet and the surface of the fabricated structure (Fig. 10d). Subsequently, the arc was extinguished, and the tip of the wire was heated owing to Joule heating (Fig. 10e). Finally, the wire was snapped off, and the arc was simultaneously generated (Fig. 10f).

Figure 11 demonstrates the appearance of the single and multilayer structures fabricated for heat input of 1.17 kJ/cm under different gases. The number of layers was 1, 2, 3, 5, 11, and 31. For Ar gas, the metal droplets were discontinuously formed on the substrate during the 1st layer deposition. However, as the number of layers increased to more than three, the structure exhibited a uniform surface. For CO_2 gas, the first layer exhibited a uniform surface, although the 2nd and subsequent layers showed partial deterioration (humping) on the surface, as shown in Fig. 11c.

Figure 12 presents the side view of the thin-wall structures with 31 layers fabricated for the heat inputs of 1.17 kJ/cm under different gases. For Ar gas, the top face of the structure was relatively uniform. In contrast, the top face of the structure was markedly irregular under CO_2 gas.

Figure 13 depicts the variations in the heights and widths of the single and multilayer structures fabricated for the heat input of 1.17 kJ/cm under different gases. For both gases, the heights were almost the same and increased linearly with an increase in the number of layers. Further, as the number of layers increased to more than five, the increase in the width gradually increased. However, when the number of layers increased, the variations in the height and width increased under CO_2, whereas decreased under Ar gas.

Figure 14 compares the surface profiles with the increase in the number of layers for the heat input of 1.17 kJ/cm under Ar gas. The first layer was significantly irregular, indicating a poor surface quality. However, the flatness of the surface improved with an increase in the number of layers. The heights of the 5th and subsequent layers are uniform. This indicates that the use of Ar gas as the shield gas is advantageous for the high surface quality of the multilayer structure.

Figure 15 presents the side face of the thin-wall structures with 31 layers fabricated for the heat input of 1.17 kJ/cm under different gases. WAAM is based on the layer-upon-layer process, such that the boundaries in adjacent layers are formed, which is known as the stair stepping effect [27]. This is inevitably produced on the side face of the fabricated structure. For Ar gas, the stair steps can be clearly observed. However, distinct stair steps could not be observed under CO_2 gas.

Figure 16 compares the surface roughness of the side face of the thin-wall structures fabricated for the heat input of 1.17 kJ/cm under different gases. The surface roughness was lower under Ar gas than under CO_2 gas. Moreover, the variation in the surface roughness was lower under Ar gas. This indicates that Ar gas is advantageous for improving the surface quality of multilayer structures.

3.4. Metal transfer behavior under different heat inputs

Figure 17 displays the metal transfer behavior at different heat inputs under Ar gas. These images were observed 13 ms after the short-circuit phase in the deposition of the 31st layer. The droplet radii were

almost the same for both heat inputs. At a higher heat input, the arc blew to a wider area toward the traveling direction. Furthermore, the volume of the molten pool is larger at a higher heat input. Further, the frequency of the short-circuit was 17.74 Hz for heat input of 1.17 kJ/cm, and 35.41 Hz for heat input of 2.56 kJ/cm.

Figure 18 depicts the appearance of the single and multilayer structures fabricated at the heat input of 2.56 kJ/cm under Ar gas. The 1st and 2nd layers showed a nonuniform surface, but the subsequent layers exhibited a uniform surface.

Figure 19 demonstrated the side view of the thin-wall structures with 31 layers fabricated for the heat input of 2.56 kJ/cm under Ar gas. The deterioration of the top face at the edge area was observed because of the overflow of the molten metal.

Figure 20 shows the variations in the heights and widths of the single and multilayer structures fabricated at different heat inputs under Ar gas. It should be noted that the value of the width excludes the overflow of molten metal. The heights were almost the same for both heat inputs. However, the widths were larger for heat input of 2.56 kJ/cm, than for a heat input of 1.17 kJ/cm. The variations in the heights and widths decreased with an increase in the number of layers.

Figure 21 presents the side face of the thin-wall structures with 31 layers fabricated for heat inputs of 2.56 kJ/cm under Ar gas. The adjacent layers had no uniform boundaries, although stair steps could be observed.

Figure 22 compares the surface roughness of the side face of the thin-wall structures fabricated at different heat inputs under Ar gas. The surface roughness increased with an increase in heat input indicating that a lower heat input is advantageous for improving the surface quality of multilayer structures.

Figure 23 displays the results of the SEM-EDS analysis for the surface of the first layer fabricated at the heat input of 1.17 kJ/cm under Ar gas. Table 3 lists the chemical composition of the surface of the 1st layer and substrate, and it should be noted that the chemical composition was obtained through the quantitative analysis of the whole area of the SEM image (Fig. 23b). The oxide and iron contents can be observed in the EDS element mapping. Moreover, the oxygen content of the surface of the 1st layer was almost 10 times larger than that of the substrate (Table 3).

Table 3
Chemical composition of the surface on the 1st layer and substrate.

Element [wt%]	1st layer	Substrate
C K	10.04	10.04
O K	22.26	2.18
Si K	0.11	0.22
Mn K	0.75	0.77
Fe K	66.84	86.79

Discussion

4.1. Classification of metal transfer mode

In the GMAW process, there are two types of metal transfer modes: short-circuiting and free-flight [16, 17]. In this study, a short circuit transfer mode was observed under all conditions.

4.2. Influence of metal transfer behavior during single and multilayer deposition on geometry and surface roughness

The influence of the metal transfer behavior during single and multilayer deposition under Ar gas on the geometry and surface roughness of the single and multilayer structures is described. It is known that Ar gas is not suitable for welding steel because it cannot provide the desired arc stability and weld bead characteristics [28]. This is because the cathode spots can be formed on a metal oxide, such that an insufficient supply of oxygen to the molten pool results in a reduction in the arc stability [29]. As shown in Fig. 6, the arc cannot generate stably after the short circuit phase in the 1st layer deposition. The tip of the wire is heated owing to Joule heating, and the wire subsequently snaps off. These cycles produce discontinuous metal droplets on the substrate, which results in poor surface quality, as shown in Fig. 11a. However, the flatness of the surface as well as the variations in current and voltage improve with an increase in the number of layers, as shown in Figs. 5 and 14. This is influenced by the difference in the arc stability. Further, as shown in Fig. 7, the arc blows to the surface of the molten pool in the traveling direction. This allows the molten pool to constantly form in front of the wire. Thus, a droplet with a large radius is stably sucked into the molten pool during the short circuit phase and spreads to the fabricated surface after droplet detachment. This enables the reduction of surface irregularities. This stable metal transfer behavior affected the surface roughness. The boundary between the adjacent layers becomes uniform, which leads to a lower surface roughness, as shown in Figs. 15 and 16. The improvement in the arc stability may be achieved by the oxide layer formed on the surface during the building. In addition, the oxygen content of the surface of the 1st layer was almost 10 times larger than that of the substrate, as listed in Table 3. In the WAAM process, the shielding gas is supplied through the torch. Furthermore, the

shielding effect appears to be weak under multilayer fabrication, which promotes the oxidation of the surface of the fabricated structure.

4.3. Influence of metal transfer behavior under different shielding gases on geometry and surface roughness

The influence of the metal transfer behavior under different shielding gases on the geometry and surface roughness of single and multilayer structures is described. In contrast to Ar gas, the surface quality as well as the variations in the current and voltage deteriorate with an increase in the number of layers under CO_2 gas, as depicted in Figs. 9 and 11b. CO_2 gas promotes the transfer of the small droplet to the molten pool, and the arc blows to a narrow area just below the wire, as shown in Fig. 8. During the fabrication, the arc blew to the surface of the molten pool in the traveling direction, as shown in Fig. 10 and thereafter, the arc blew instantaneously from the surface of the molten pool to the previously fabricated surface. This is because the cathode spot transfers from the molten pool to the previously fabricated surface to find the shortest path according to the principle of minimum voltage [30]. Therefore, the molten pool cannot be formed in front of the wire before the short circuit phase. This allows a short circuit between the droplet and the surface of the fabricated structure. It has been reported that the electromagnetic force and surface tension of the droplet have a significant influence on the stable metal transfer in the short-circuit phase [31]. It was considered that the temperature of the metal bridge decreased owing to the heat diffusion to the fabricated structure, which resulted in an increase in the surface tension. This interrupts the neck from the metal bridge. As a result, the wire was snapped off by Joule heating. This phenomenon is often observed during the fabrication on the hump surface. By repeating these cycles, the waviness of the top face of the multilayer structure increases, as shown in Fig. 12b. Therefore, the molten pool was formed and solidified randomly in the height direction leading to distinct stair steps on the side face of the multilayer structure and an increase in the surface roughness, as shown in Figs. 15 and 16.

4.4. Influence of metal transfer behavior under different heat inputs on geometry and surface roughness

The influence of the metal transfer behavior under different heat inputs on the geometry and surface roughness of single and multilayer structures is described. The higher heat input improved the surface quality of the single and multilayer layers. The electromagnetic force increases with an increase in current. It can be deduced that a higher electromagnetic force promotes the confinement of the metal bridge, which results in stable metal transfer. However, excessive heat input decreases the surface quality of the thin-wall structure owing to the overflow of the molten metal from the top face. In addition, the frequency of the short circuit increases at a higher heat input, which increases the volume of the molten pool, as shown in Fig. 17. It was considered that the overflow of the molten metal was caused by an increase in the volume of the molten pool and a decrease in the surface tension due to heat accumulation. It appears that the large volume of the molten pool leads to an increase in the remelting area resulting in unclear stair steps between the adjacent layers of the side face of the thin-wall structure,

as displayed in Fig. 21. As a result, the surface roughness increases with an increase in the heat input, as shown in Fig. 22.

Conclusions

This study focused on the GMAW-based WAAM process. The influence of the metal transfer behavior of mild steel under different shielding gases and heat inputs on the geometry and surface roughness of the fabricated structure was investigated. The chemical composition of the fabricated surface was analyzed using EDS. The major results obtained are as follows:

1. For a heat input of 1.17 kJ/cm under Ar gas, a higher geometric accuracy of the thin-wall structure was obtained without interlayer cooling.
2. For Ar gas, an arc blows widely in the traveling direction, which leads to stable short circuit metal transfer. This enables the reduction of surface irregularities on the fabricated structure.
3. The short circuit between the metal droplet and the fabricated surface, where the molten pool is insufficiently formed leads to hump formation.
4. The molten metal overflows from the top face of the thin-wall structure for a heat input of 2.56 kJ/cm, which results in a reduction in geometric accuracy.
5. The surface roughness increases with an increase in heat input. Ar gas enables a lower surface roughness of the thin-wall structure than that of CO_2 gas.
6. Stable fabrication under Ar gas is achieved by the formation of an oxide layer on the fabricated surface.

The results of this study demonstrate that the use of Ar as a shielding gas can be an effective approach for achieving higher geometric accuracy of the multilayer structure. In future work, the effect of the thickness of the oxide layer on the arc stability will be evaluated through a detailed quantitative analysis. The results will be linked to the metal transfer behavior for a comprehensive understanding of the WAAM process.

Declarations

Compliance with Ethical Standards

Ethical approval Not applicable.

Consent to participate Not applicable.

Consent to publish All authors consented to the publication.

Authors' contributions MY organized all the data and wrote the manuscript. RK investigated the fabrication characteristics of single and multilayer structures. TF evaluated the surface quality of the fabricated structure and observed the metal transfer behavior. SA analyzed the fabricated surface using

energy-dispersive X-ray spectroscopy (EDS). AH supervised all the research and analysis. All authors read and approved the final manuscript.

Funding This work was partially supported by Mitani Foundation for Research and Development and Amada Foundation.

Competing interests All authors declare that they have no competing.

Availability of data and materials All data generated or analyzed during this study are included in this published article.

References

1. Li JZ, Alkahari MR, Rosli NAB, Hasan R, Sudin MN, Ramli FR (2019) Review of wire Arc Additive Manufacturing for 3D metal printing. Int J Autom Technol 13:346–353. https://doi.org/10.20965/ijat.2019.p0346
2. Ding D, Pan Z, Cuiuri D, Li H (2015) Wire-feed additive manufacturing of metal components: technologies, developments and future interests. Int J Adv Manuf Technol 81:465–481. https://doi.org/10.1007/s00170-015-7077-3
3. Karayel E, Bozkurt Y (2020) Additive manufacturing method and different welding applications. J Mater Res Technol 9:11424–11438. https://doi.org/10.1016/j.jmrt.2020.08.039
4. Kumar M, Sharma A, Mohanty UK, Kumar SS (2019) Advances in welding technologies for process development: additive manufacturing with welding, 1st edn. CRC Press, Boca Raton, pp 77–100. https://doi.org/10.1201/9781351234825
5. Rafieazad M, Ghaffari M, Vahedi Nemani AV, Nasiri A (2019) Microstructural evolution and mechanical properties of a low-carbon low-alloy steel produced by wire arc additive manufacturing. Int J Adv Manuf Technol 105:2121–2134. https://doi.org/10.1007/s00170-019-04393-8
6. Yildiz AS, Davut K, Koc B, Yilmaz O (2020) Wire arc additive manufacturing of high-strength low alloy steels: study of process parameters and their influence on the bead geometry and mechanical characteristics. Int J Adv Manuf Technol 108:3391–3404. https://doi.org/10.1007/s00170-020-05482-9
7. Liu J, Xu Y, Ge Y, Hou Z, Chen S (2020) Wire and arc additive manufacturing of metal components: a review of recent research developments. Int J Adv Manuf Technol 111:149–198. https://doi.org/10.1007/s00170-020-05966-8
8. Martina F, Roy MJ, Szost BA, Terzi S, Colegrove PA, Williams SW, Withers PJ, Meyer J, Hofmann M (2016) Residual stress of as-deposited and rolled wire + arc additive manufacturing Ti–6Al–4V components. Mater Sci Technol 32:1439–1448. https://doi.org/10.1080/02670836.2016.1142704
9. Busachi A, Erkoyuncu J, Colegrove P, Martina F, Ding J (2015) Designing a WAAM based manufacturing system for defence applications. Procedia CIRP Proc CIRP 37:48–53. https://doi.org/10.1016/j.procir.2015.08.085

10. IvánTabernero I, Paskual A, Álvarez P, Suárez A (2018) Study on Arc Welding processes for High Deposition Rate Additive Manufacturing. Procedia CIRP Proc CIRP 68:358–362. https://doi.org/10.1016/j.procir.2017.12.095
11. Xiong J, Li Y, Li R, Yin Z (2018) Influences of process parameters on surface roughness of multi-layer single-pass thin-walled parts in GMAW-based additive manufacturing. J Mater Process Technol 252:128–136. https://doi.org/10.1016/j.jmatprotec.2017.09.020
12. Prado-Cerqueira JL, Camacho AM, Diéguez JL, Rodríguez-Prieto Á, Aragón AM, Lorenzo-Martín C, Yanguas-Gil Á (2018) Analysis of favorable process conditions for the manufacturing of thin-wall pieces of mild steel obtained by wire and Arc Additive Manufacturing (WAAM). Materials (Basel) 11:1449–1466. https://doi.org/10.3390/ma11081449
13. Jurić I, Garašić I, Bušić M, Kožuh Z (2019) Influence of shielding gas composition on structure and mechanical properties of wire and arc additive manufactured Inconel 625. JOM 71:703–708. https://doi.org/10.1007/s11837-018-3151-2
14. Silwal B, Nycz A, Masuo CJ, Noakes MW, Marsh D, Vaughan D (2020) An experimental investigation of the effectiveness of Ar-CO_2 shielding gas mixture for the wire arc additive process. Int J Adv Manuf Technol 108:1285–1296. https://doi.org/10.1007/s00170-020-05395-7
15. International Institute of Welding (1976) Classification of metal transfer, IIW Doc. XII-636-76
16. Scotti A, Ponomarev V, Lucas W (2012) A scientific application oriented classification for metal transfer modes in GMA welding. J Mater Process Technol 212:1406–1413. https://doi.org/10.1016/j.jmatprotec.2012.01.021
17. Scotti A, Ponomarev V, Lucas W (2014) Interchangeable metal transfer phenomenon in GMA welding: features, mechanisms, classification. J Mater Process Technol 214:2488–2496. http://dx.doi.org/10.1016/j.jmatprotec.2014.05.022
18. Teixeira GS, Mazzaferro JAE (2019) GMA welding metal transfer mode study by high-speed imaging and electrical signal acquisition. J Braz Soc Mech Sci Eng 41:315. https://doi.org/10.1007/s40430-019-1814-8
19. Wu B, Ding D, Pan Z, Cuiuri D, Li H, Han J, Fei Z (2017) Effects of heat accumulation on the arc characteristics and metal transfer behavior in Wire Arc Additive Manufacturing of Ti6Al4V. J Mater Process Technol 250:304–312. https://doi.org/10.1016/j.jmatprotec.2017.07.037
20. Ríos S, Colegrove PA, Williams SW (2019) Metal transfer modes in plasma Wire + Arc additive manufacture. J Mater Process Technol 264:45–54. https://doi.org/10.1016/j.jmatprotec.2018.08.043
21. Liang Z, Jinglong L, Yi L, Jingtao H, Chengyang Z, Jie X, Dong C (2018) Characteristics of metal droplet transfer in wire-arc additive manufacturing of aluminum alloy. Int J Adv Manuf Technol 99:1521–1530. https://doi.org/10.1007/s00170-018-2604-7
22. Cai X, Fan C, Lin S, Yang C, Hu L, Ji X (2017) Effects of shielding gas composition on arc behaviors and weld formation in narrow gap tandem GMAW. Int J Adv Manuf Technol 91:3449–3456. https://doi.org/10.1007/s00170-017-9990-0

23. Thakur A, Gebrelibanos H, Gabrey T (2019) Arc welding process selection through a quality and costs. Int J Curr Eng Technol 9:383–394. DOI:https://doi.org/10.14741/ijcet/v.9.3.6
24. Cunningham CR, Flynn JM, Shokrani A, Dhokia V, Newman ST (2018) Invited review article: strategies and processes for high quality wire arc additive manufacturing. Addit Manuf 22:672–686. https://doi.org/10.1016/j.addma.2018.06.020
25. Dinovitzer M, Chen X, Laliberte J, Huang X, Frei H (2019) Effect of wire and arc additive manufacturing (WAAM) process parameters on bead geometry and microstructure. Addit Manuf 26:138–146. https://doi.org/10.1016/j.addma.2018.12.013
26. Xiong J, Li YJ, Yin ZQ, Chen H (2018) Determination of surface roughness in wire and arc additive manufacturing based on laser vision sensing. Chin J Mech Eng 31:1–7. https://doi.org/10.1186/s10033-018-0276-8
27. Alimardani M, Fallah V, Iravani-Tabrizipour M, Khajepour A (2012) Surface finish in laser solid freeform fabrication of an AISI 303L stainless steel thin wall. J Mater Process Technol 212:113–119. https://doi.org/10.1016/j.jmatprotec.2011.08.012
28. Davies AC (1993) The science and practice of welding, 10th edn. Cambridge University Press, Cambridge, pp 114–121
29. Kah P, Martikainen J (2013) Influence of shielding gases in the welding of metals. Int J Adv Manuf Technol 64:1411–1421. https://doi.org/10.1007/s00170-012-4111-6
30. Chen YB, Feng JC, Li LQ, Li Y, Chang S (2013) Effects of welding positions on droplet transfer in CO_2 laser-MAG hybrid welding. Int J Adv Manuf Technol 68:1351–1359. https://doi.org/10.1007/s00170-013-4926-9
31. Anzehaee MM, Haeri M (2011) Estimation and control of droplet size and frequency in projected spray mode of a gas metal arc welding (GMAW) process. ISA Trans 50:409–418. https://doi.org/10.1016/j.isatra.2011.02.004

Figures

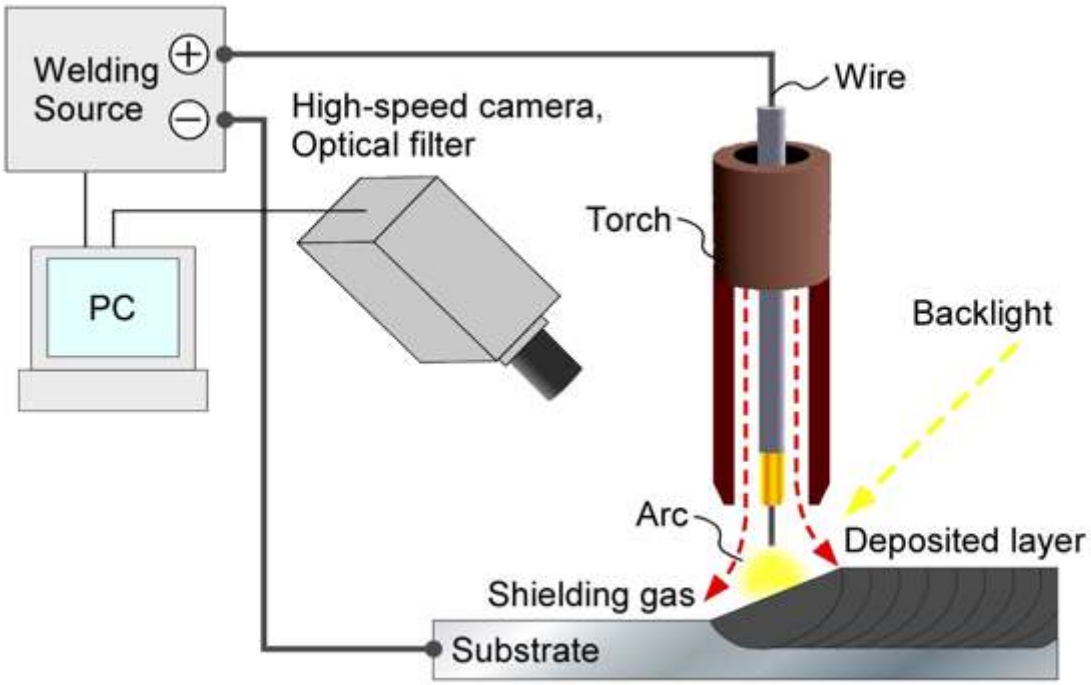

Figure 1

Schematic of the experimental setup.

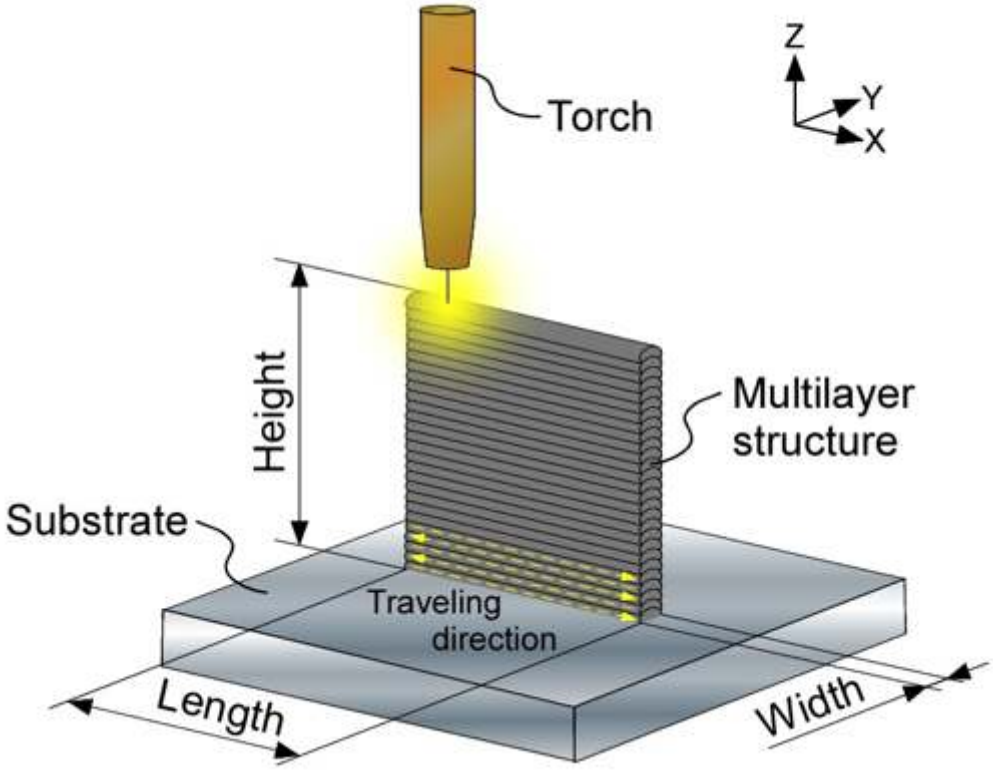

Figure 2

Schematic of the traveling path.

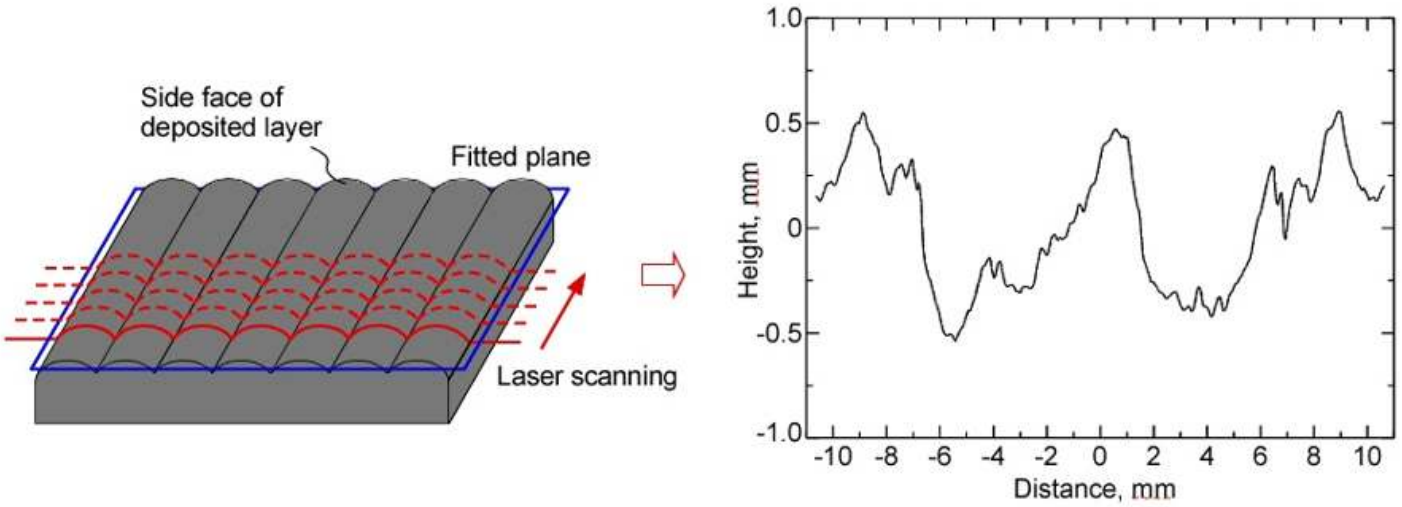

Figure 3

Schematic of the surface roughness measurement.

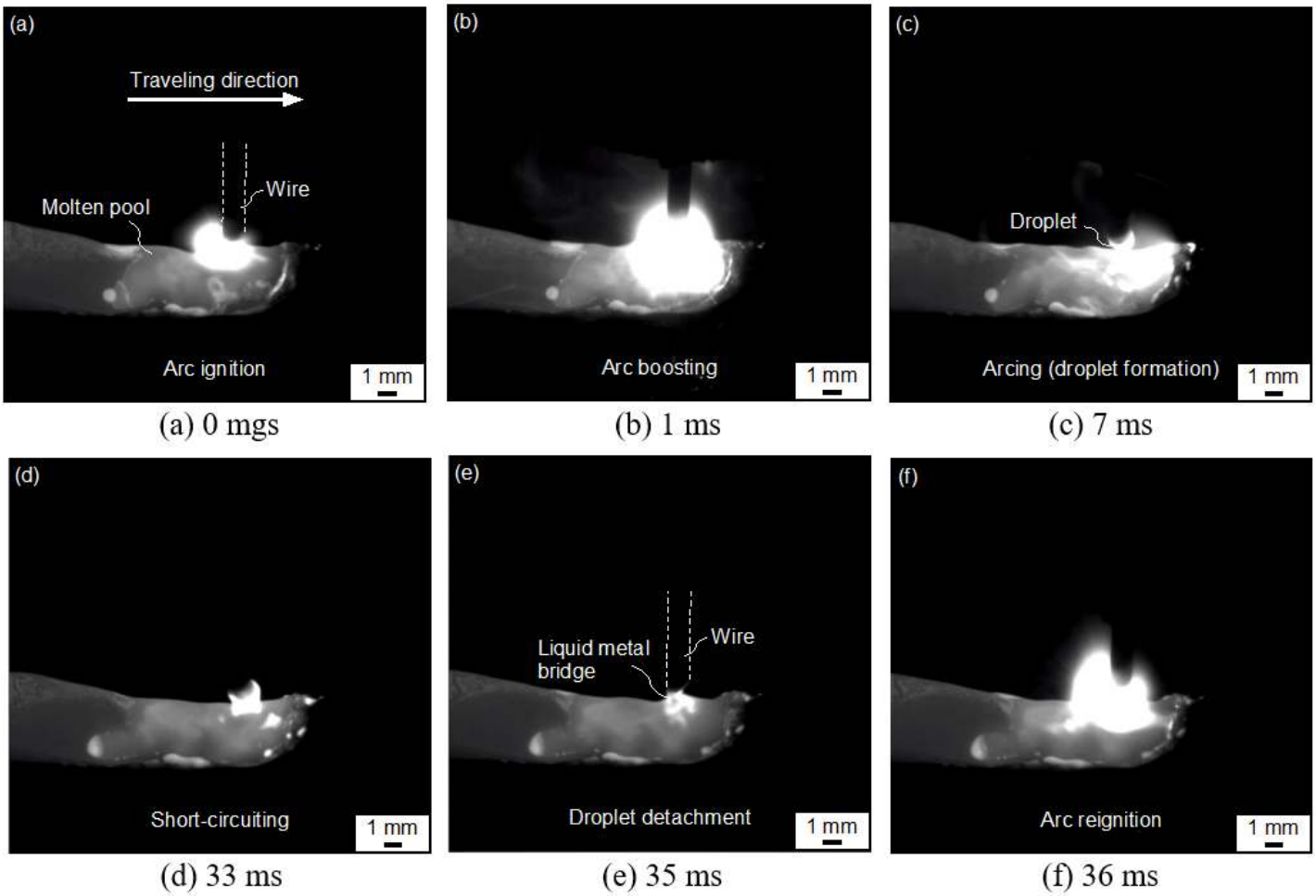

Figure 4

One cycle of the metal transfer behavior during the fabrication.

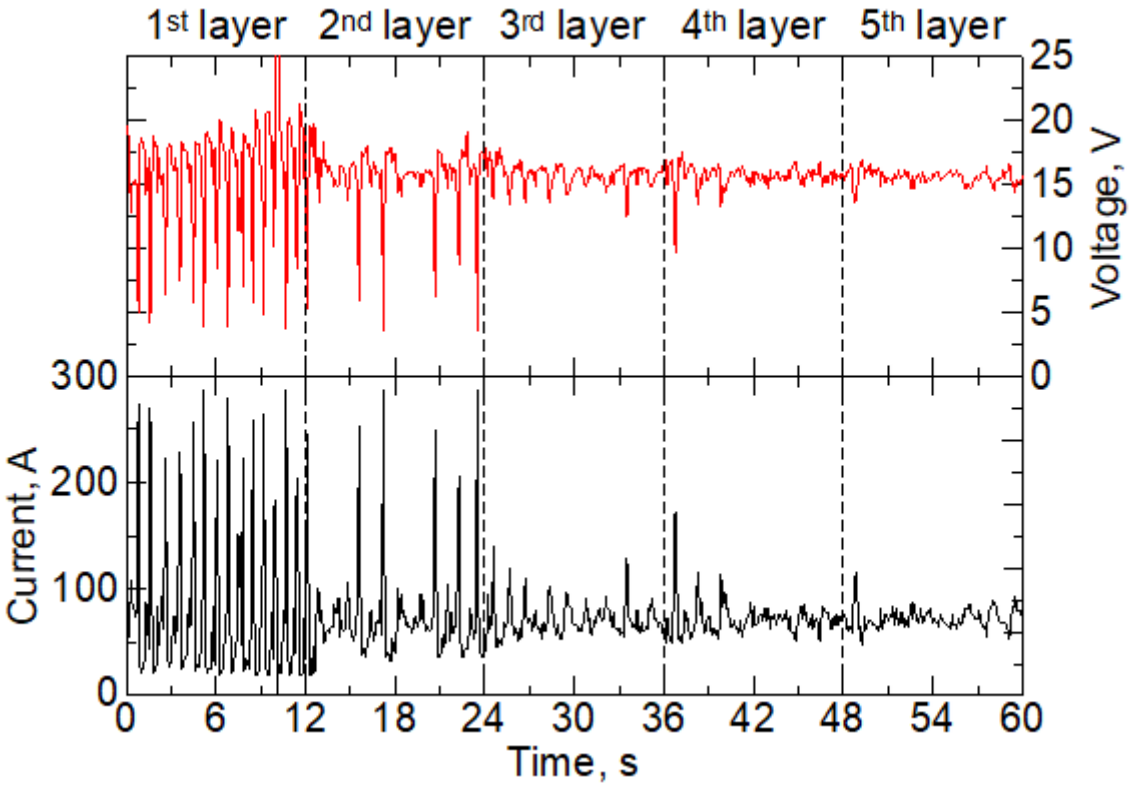

Figure 5

Variations in the current and voltage during the fabrication for five layers for heat input of 1.17 kJ/cm under Ar gas.

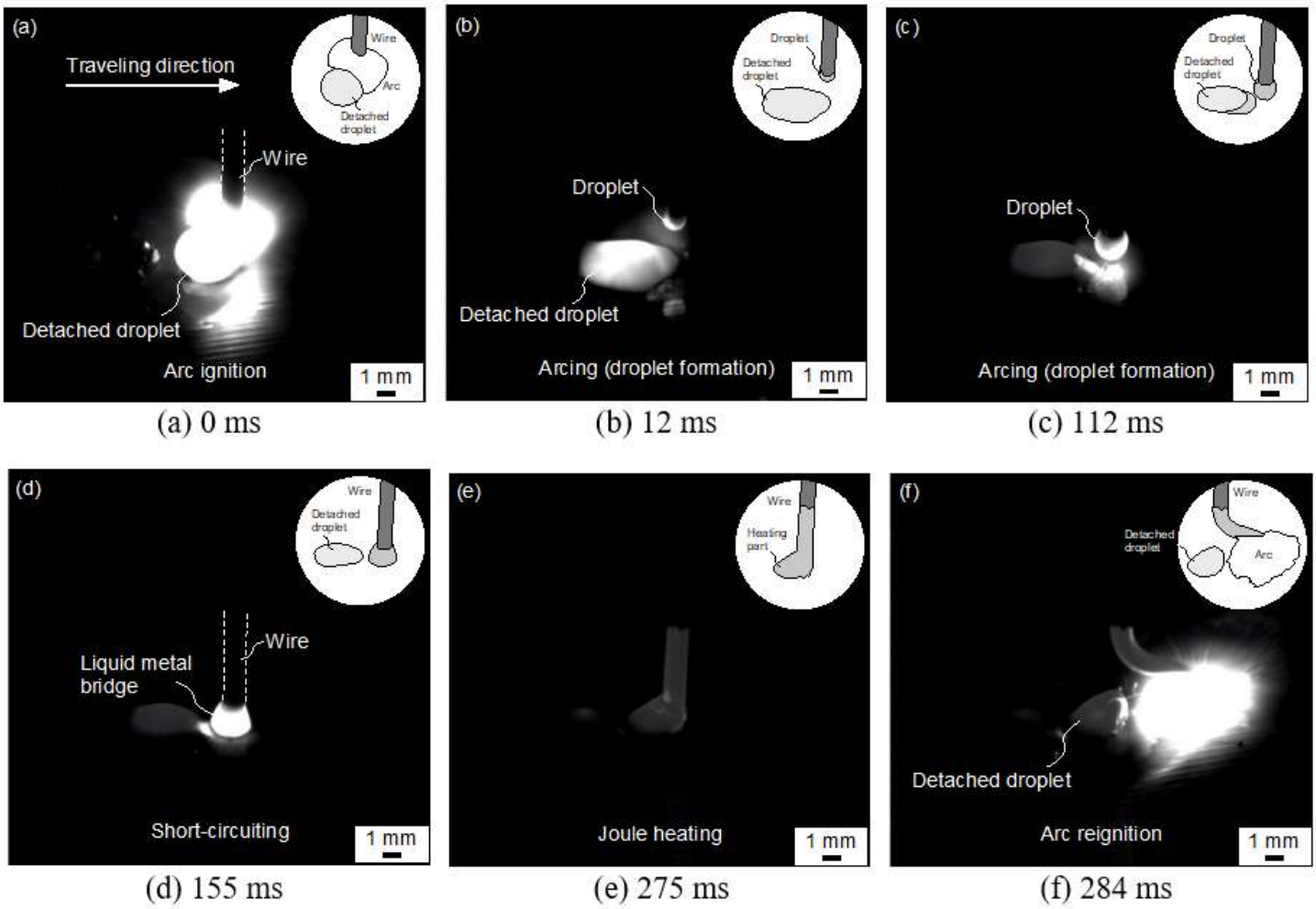

Figure 6

The metal transfer behavior in the 1st layer deposition for heat input of 1.17 kJ/cm under Ar gas.

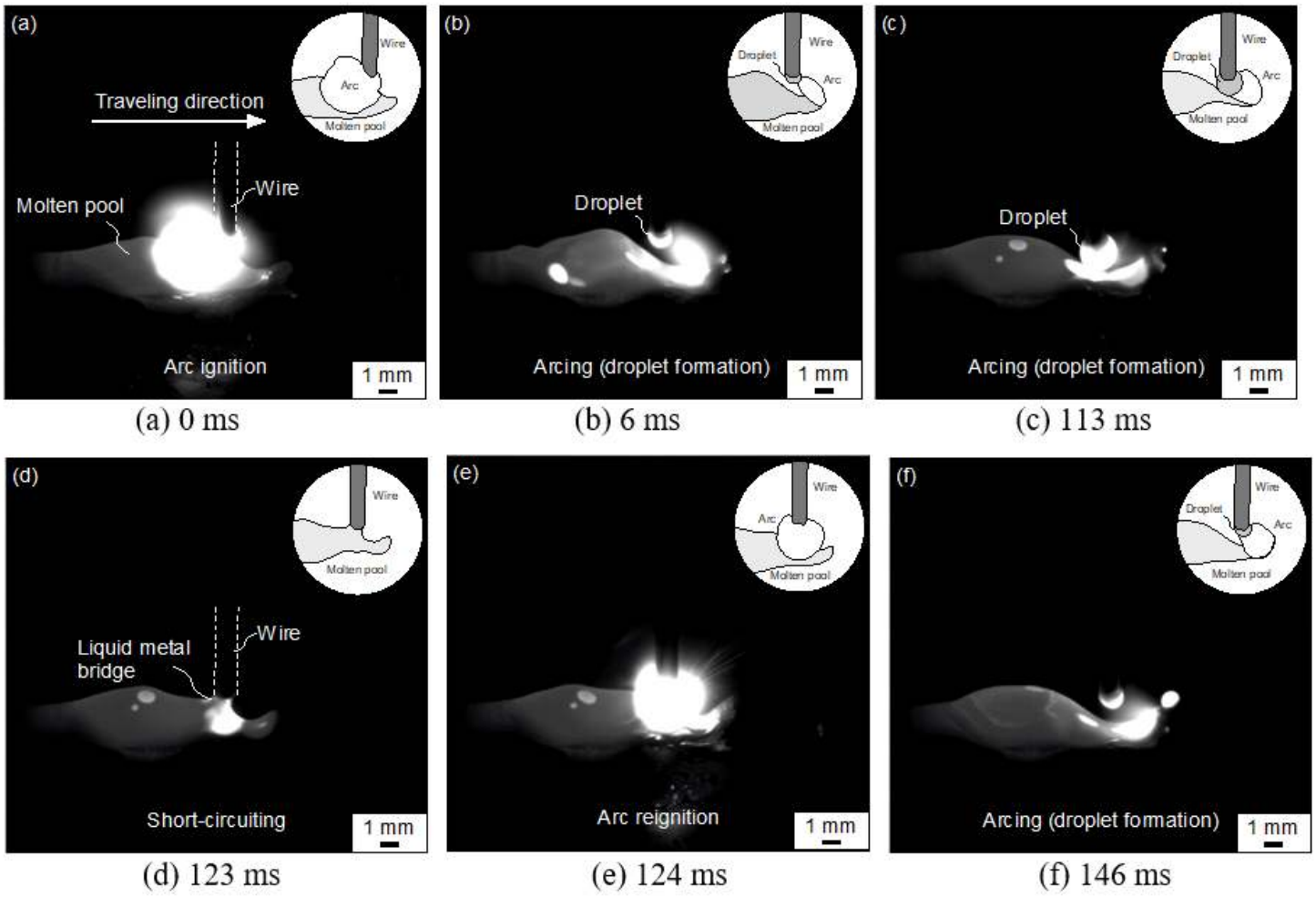

Figure 7

The metal transfer behavior in the 3rd layer deposition for heat input of 1.17 kJ/cm under Ar gas.

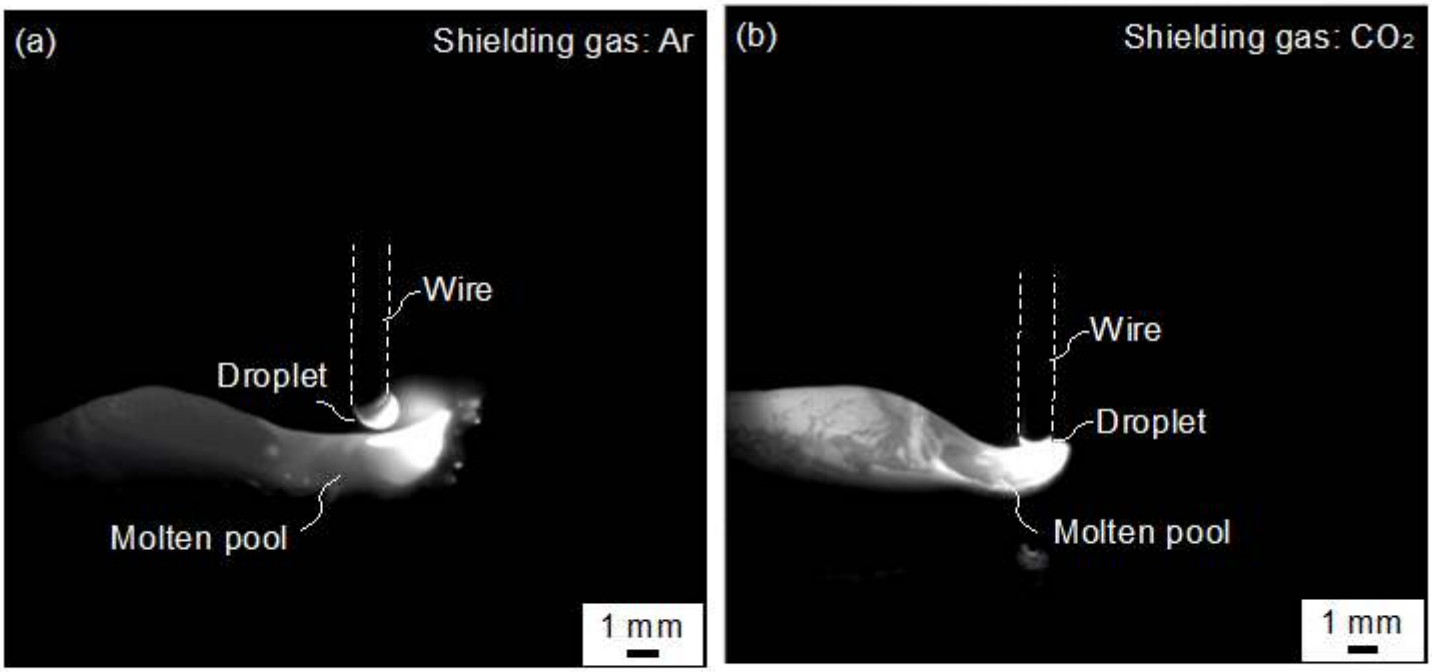

Figure 8

Comparison of the metal transfer behavior for heat input of 1.17 kJ/cm under different gases.

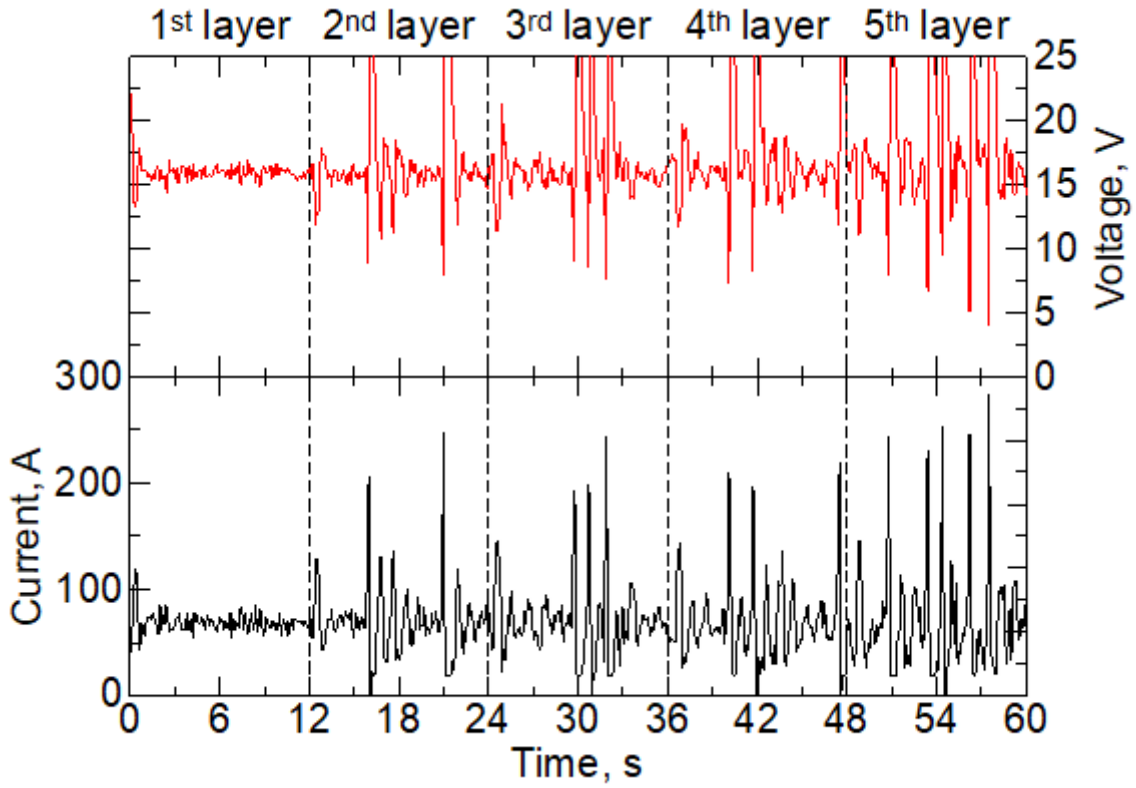

Figure 9

Variations in the current and voltage during the fabrication for five layers for heat input of 1.17 kJ/cm under CO2 gases.

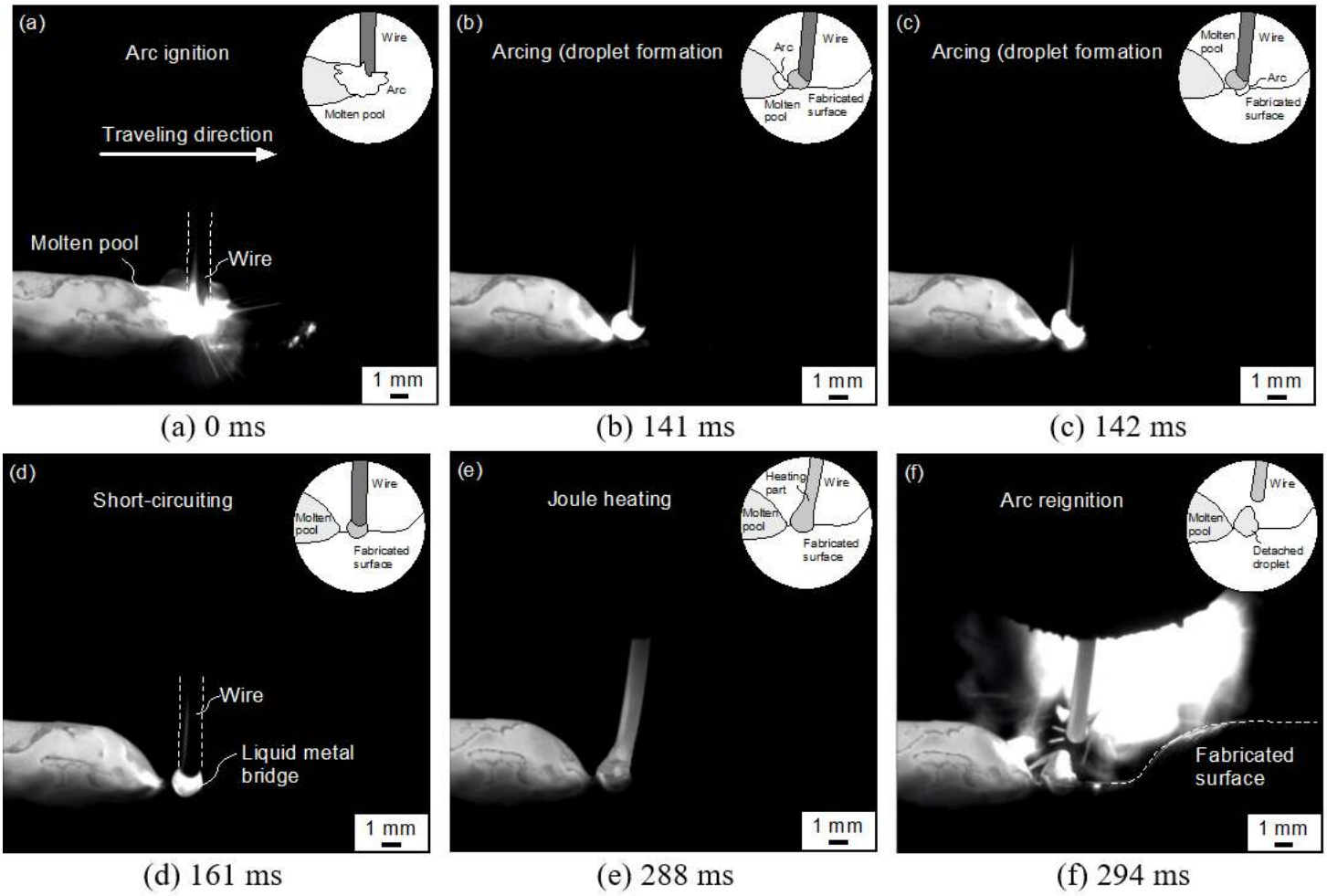

Figure 10

The metal transfer behavior in the 31st layer deposition for heat input of 1.17 kJ/cm under CO2 gas.

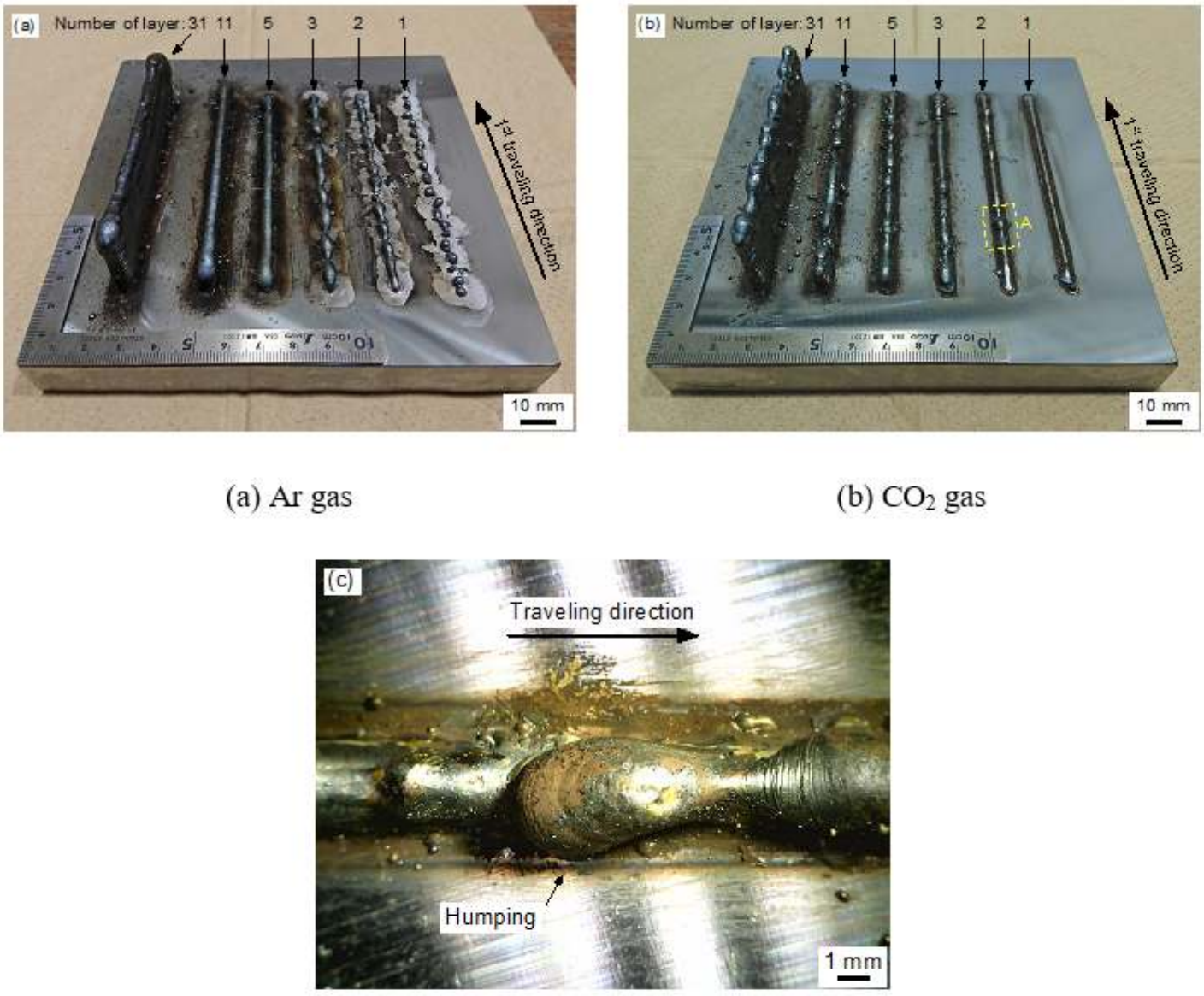

Figure 11

Appearance of the single and multilayer structures fabricated for heat input of 1.17 kJ/cm under (a) Ar gas and (b) CO2 gas. (C) Enlarged image of Area A.

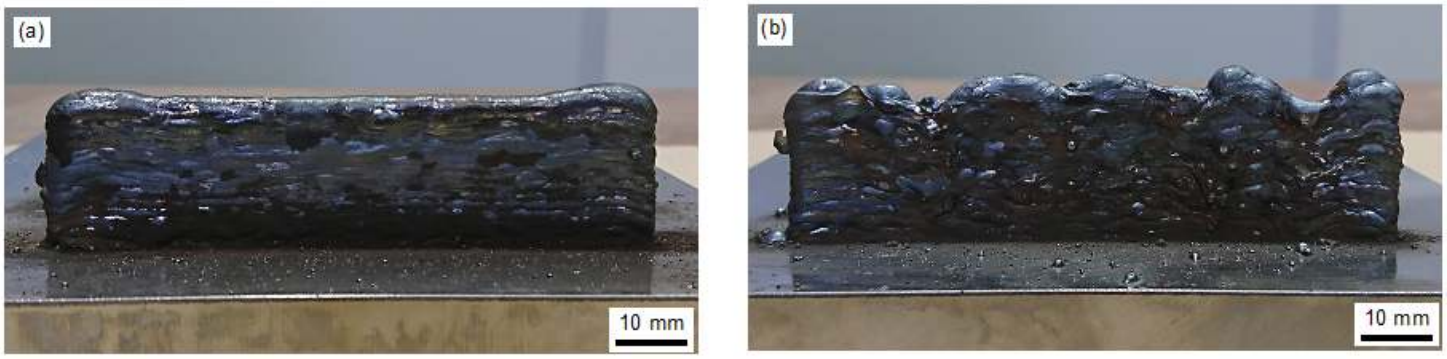

(a) Ar gas (b) CO_2 gas

Figure 12

Side view of the thin-wall structures with 31 layers fabricated for heat inputs of 1.17 kJ/cm under (a) Ar gas and (b) CO2 gas.

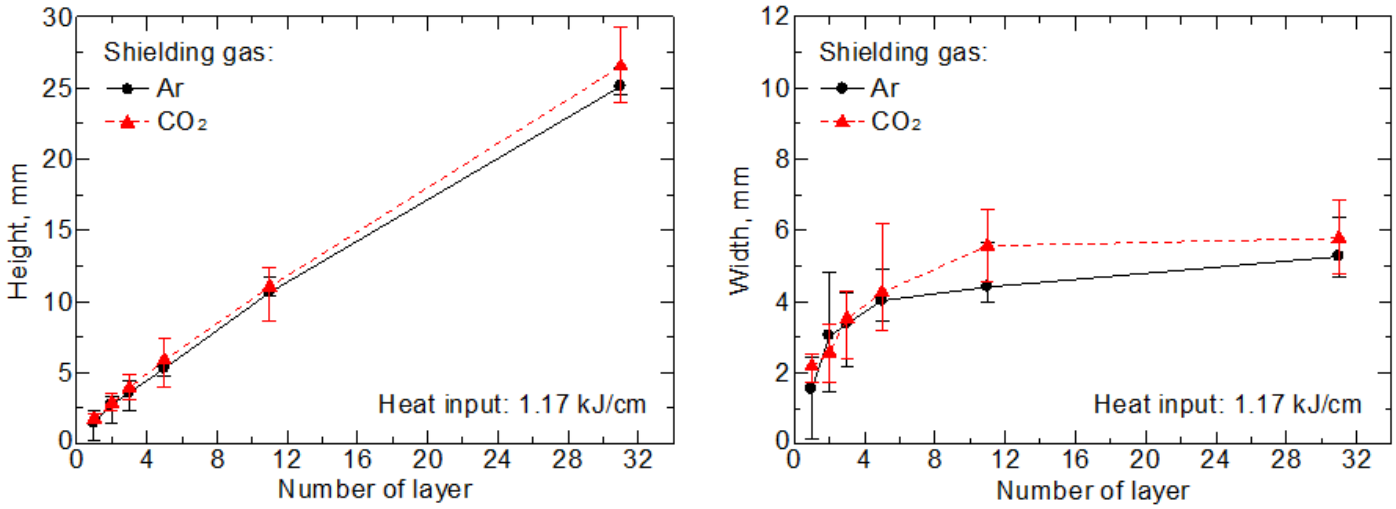

(a) Height (b) Width

Figure 13

Variation in the heights and widths of the single and multilayer structures fabricated for heat input of 1.17 kJ/cm under different gases.

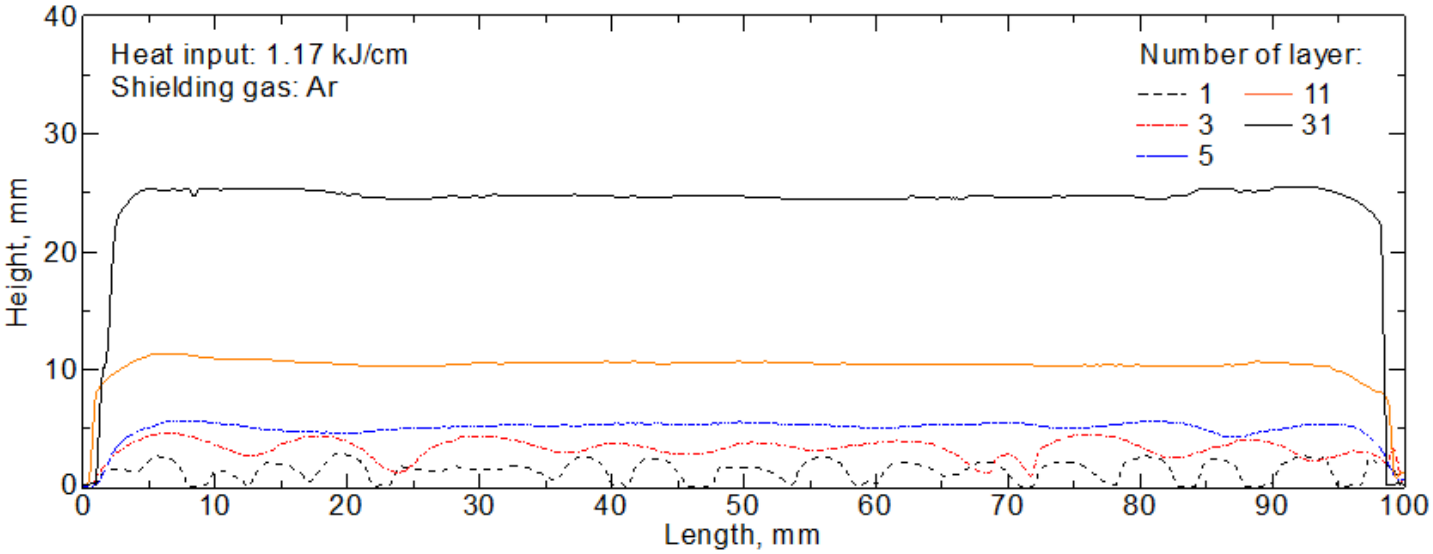

Figure 14

Variations in the surface profiles with the increase in the number of layers for heat input of 1.17 kJ/cm under Ar gas.

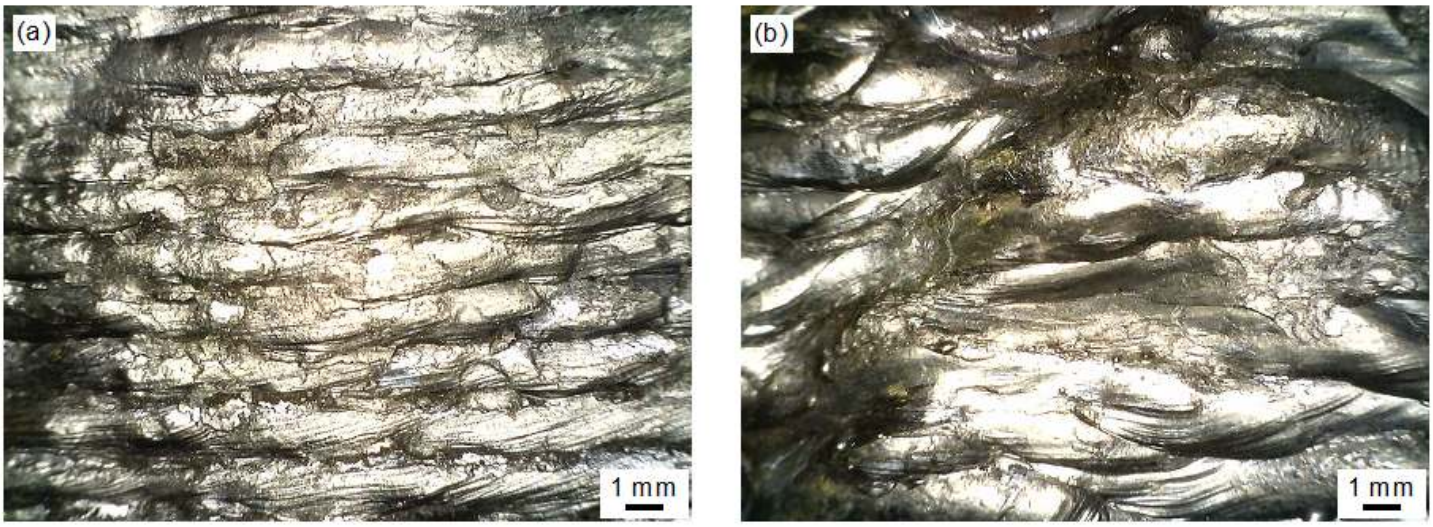

(a) Ar gas (b) CO_2 gas

Figure 15

Side surface of the thin-wall structures with 31 layers fabricated for heat input of 1.17 kJ/cm under different gases.

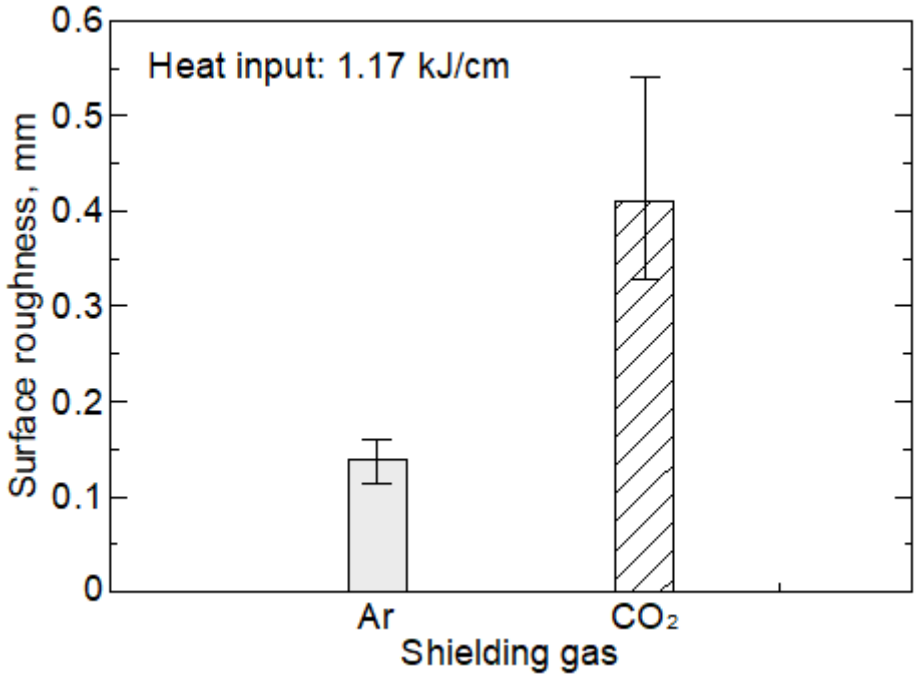

Figure 16

Comparison of the surface roughness of the side face of the thin-wall structures fabricated for heat input of 1.17 kJ/cm under different gases.

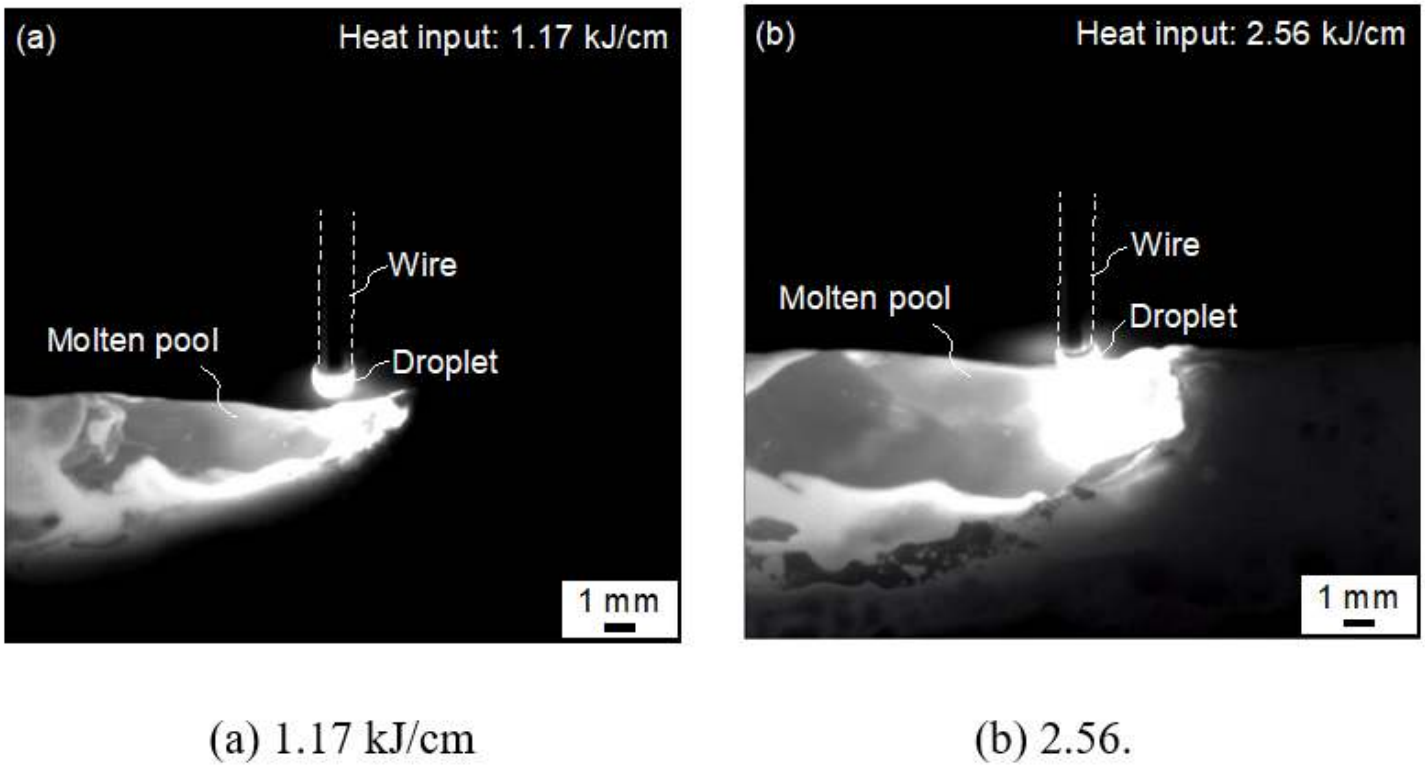

Figure 17

Comparison of the metal transfer behavior for different heat inputs under Ar gases.

Figure 18

Appearance of the single and multilayer structures fabricated for heat inputs of 2.56 kJ/cm under Ar gas.

Figure 19

Side view of the thin-wall structure with 31 layers fabricated for heat inputs of 2.56 kJ/cm under Ar gas.

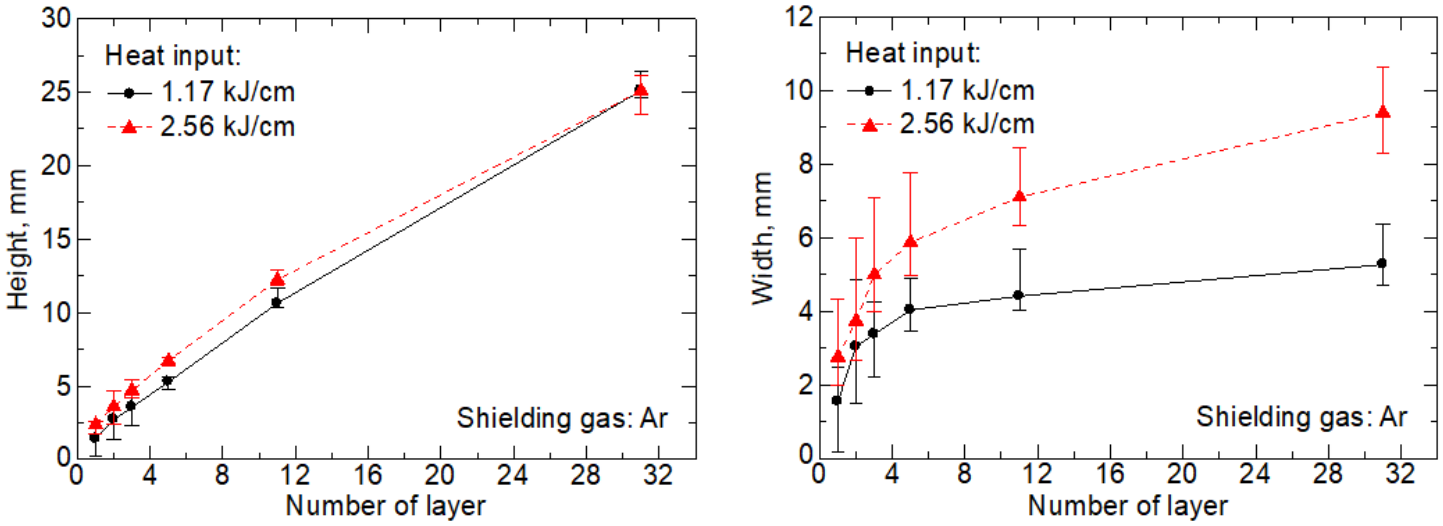

Figure 20

Variation in the heights and widths of the single and multilayer structures fabricated for different heat inputs under Ar gas.

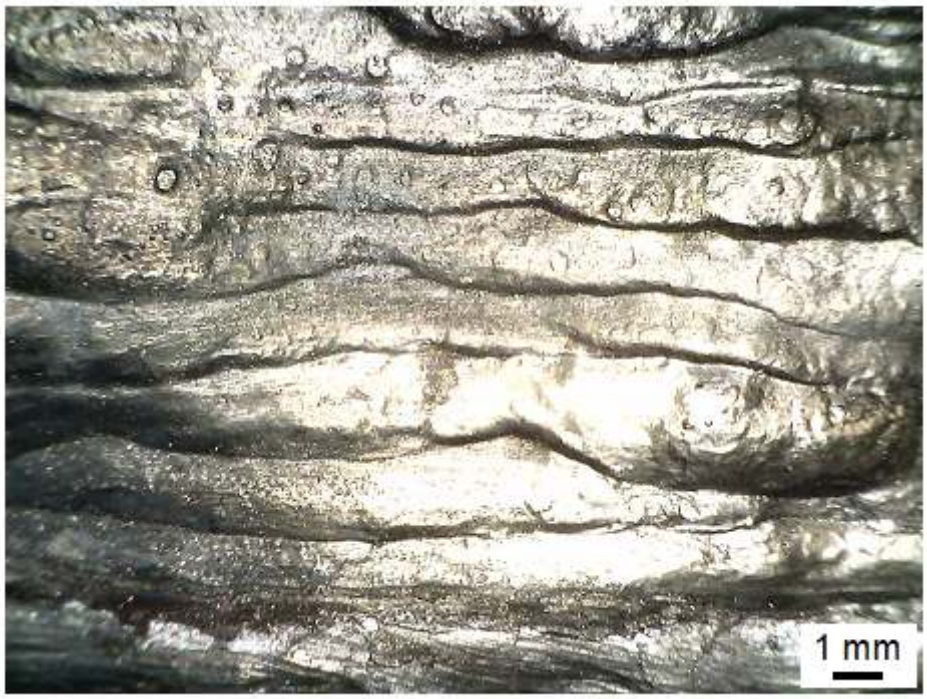

Figure 21

Side surface of the thin-wall structures with 31 layers fabricated for heat inputs of 2.56 kJ/cm under Ar gas.

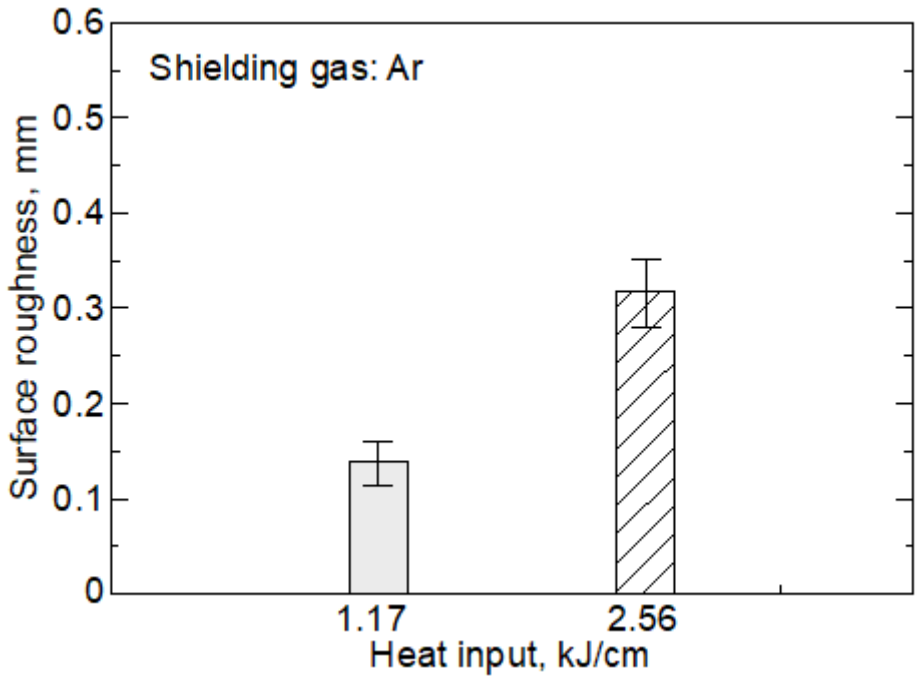

Figure 22

Comparison of the surface roughness of the side face of the thin-wall structures fabricated for heat inputs of 2.56 kJ/cm under Ar gas.

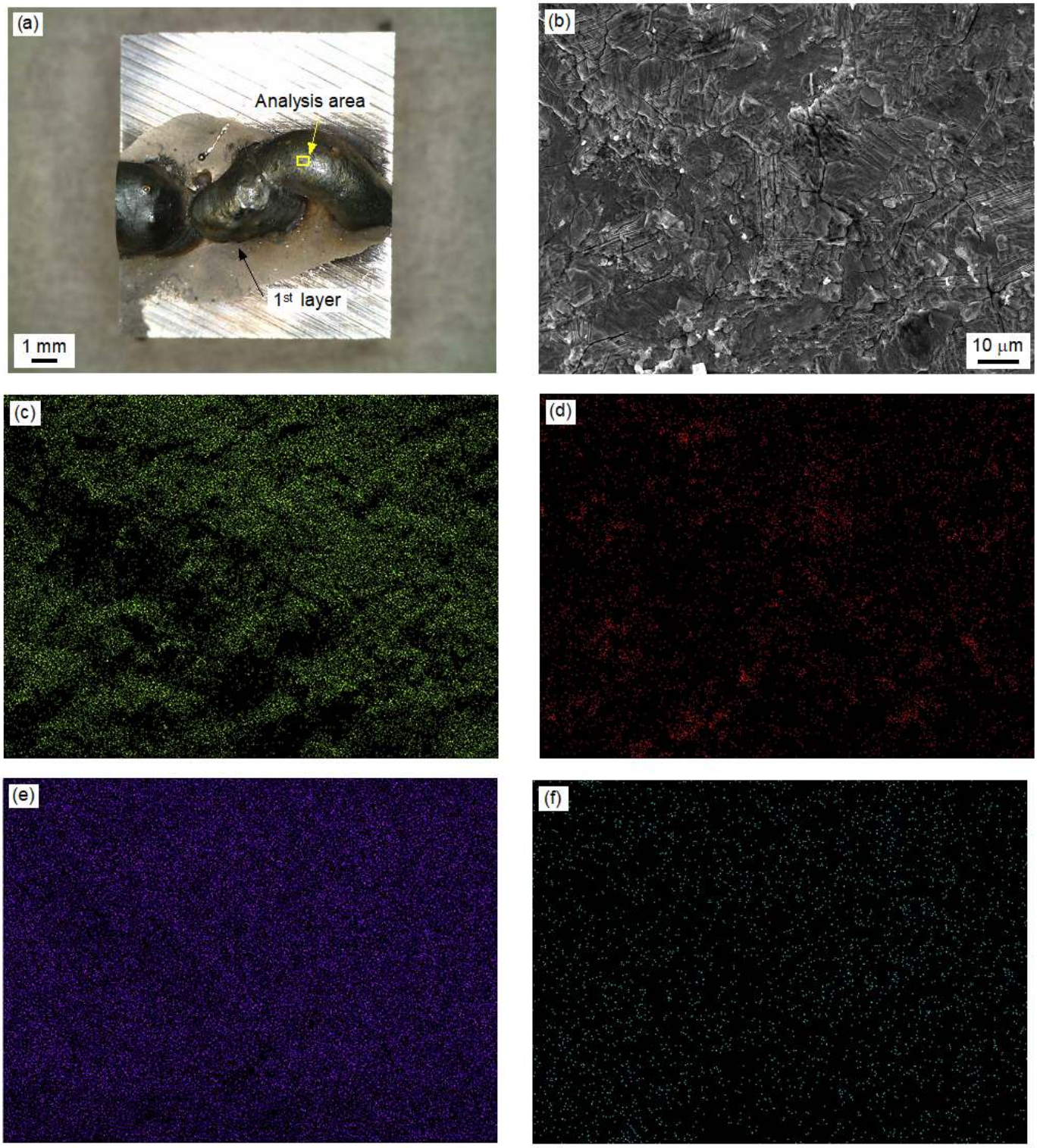

Figure 23

SEM-EDS analysis results of the first layer fabricated for heat input of 1.17 kJ/cm under Ar gas. (a) Optical microscopic image of the specimen, (b) SEM image of the analysis area, and EDS element mapping of (c) O, (d) C, (e) Fe, (f) Mn.